Research Square

Preprints are preliminary reports that have not undergone peer review.
They should not be considered conclusive, used to inform clinical practice,
or referenced by the media as validated information.

Failed table-tennis forehand drives are characterised by higher ground reaction forces and greater centre-of-pressure excursion in amateur players: a within-participant trial-level study

Mingke Han
South China Normal University
Yupeng Shen
South China Normal University
Lianzhen Ma
South China Normal University
Yufan Ding
Jinan University
Kai Xie
South China Normal University
Chaochong Deng
South China Normal University
Liang Wang
20051116@m.scnu.edu.cn
South China Normal University

Research Article

Keywords: table tennis, forehand drive, biomechanics, ground reaction force, centre of pressure, markerless motion capture, linear mixed model

Posted Date: November 5th, 2026

DOI: https://doi.org/10.21203/rs.3.rs-10308143/v1

License: This work is licensed under a Creative Commons Attribution 4.0 International License. Read Full License

Additional Declarations: No competing interests reported.

Abstract

Background

Forehand-drive errors in table tennis are often attributed to insufficient force production or racket speed. Whether successful and failed returns differ in support-limb mechanics within the same player remains unclear.

Methods

Fourteen amateur players performed standardised forehand drives against machine-fed topspin balls. Trials were classified as successful when the ball crossed the net and landed legally on the opposite half of the table; net and out-of-bounds returns were classified as failed. Ground reaction force (GRF) and combined centre-of-pressure (COP) variables were extracted from synchronised force plates. Trial-level linear mixed-effects models were fitted for 189 kinetic trials (140 successful, 49 failed), with stroke outcome as a fixed effect and participant as a random intercept. Benjamini-Hochberg false-discovery-rate correction was applied to 30 prespecified GRF/COP variables.

Results

Fifteen GRF/COP variables survived correction. Failed trials showed higher anteroposterior and vertical GRF magnitudes, greater combined-COP mean speed, path length, mediolateral fluctuation and anteroposterior/mediolateral range, and a later anteroposterior force peak. Sensitivity analyses showed that the same GRF/COP pattern generally persisted, although some short-window effects were reduced. Exploratory markerless posture-kinematic indicators were analysed separately and interpreted only as hypothesis-generating auxiliary findings.

Conclusions

In this amateur forehand-drive task, failed returns were associated with greater, not lower, support-limb force output and COP excursion. These variables may characterise support-base organisation during forehand-drive errors, but causal and training implications require longitudinal or interventional confirmation.

Background

The forehand drive is a fundamental technique for fast near-table rallying and active attack in table tennis; its stability directly affects the continuity of attack and scoring efficiency, and it has long been regarded as a cornerstone of sport-specific competence. From a biomechanical perspective, a high-quality forehand drive is not produced by the upper-limb swing alone, but results from the coordinated action of a multi-segment kinetic chain in which the lower limbs extend, the pelvis and trunk rotate, and momentum is finally transferred to the racket.

Previous studies have shown that racket speed arises from the coordinated output of multiple joint angular velocities rather than the contribution of any single joint [1], that hip kinetics (forehand) and upper-limb rotations (backhand) are both closely related to racket speed [2, 3], and that upper-limb kinetic features can distinguish the stroke technique of players at different levels [4]; analyses based on musculoskeletal modelling have further revealed the mechanical roles of the trunk, pelvis and lower limbs in the forehand stroke [5–7]. This implies that the explanation of stroke quality should not stop at the racket or the distal upper limb, but should be traced back to the support base that provides the mechanical foundation for the swing, namely the lower limbs and the pelvis-trunk segments.

To date, however, biomechanical research on the forehand drive has mainly focused on differences between “conditions” or “groups”: with respect to performance level, advanced players differ systematically from intermediate or amateur players in racket kinematics, upper-limb kinetics and lower-limb kinematics [4, 5, 8, 9]; with respect to stroke direction, straight and cross-

court strokes alter kinematic organisation as well as lumbar-pelvic motor control [6, 10, 11]; and with respect to footwork, foot-contact pattern, equipment and technique type, chasse versus one-step footwork, different foot-contact patterns, and different serving and attacking techniques produce different lower-limb loading and support mechanics [12–16], while foot-support strategy and footwork are also closely related to lower-limb loading characteristics, with implications for performance monitoring and injury-prevention research [17, 18]. Together these studies indicate that support-base mechanics are important for stroke performance, but their unit of comparison has consistently been “between individuals” or “between tasks” rather than different stroke outcomes within the same player performing the same task.

In real training and competition, the central problem facing a player is not “which technique is better” but “why the same attacking stroke sometimes yields a successful return and sometimes a failed one”. Because performance level, anthropometric characteristics and individual motor-control strategies themselves substantially affect stroke kinematics [19], between-individual or between-condition comparisons cannot easily isolate these confounders; by contrast, comparing successful and failed trials within the same participant performing the same standardised task largely controls for between-individual differences and thus more directly reveals the mechanical features associated with stroke outcome. This trial-as-unit analytical approach also echoes recent developments in trial-level table-tennis trajectory data and motion-recognition research [20].

Performance in racket sports often depends on the matching of speed, timing and kinetic-chain transfer rather than on force or velocity peaks alone [21]. It can therefore be inferred that the magnitude and timing of the ground reaction force (GRF), which reflects the support base, together with the centre-of-pressure (COP) trajectory, which reflects whole-body balance regulation, may be sensitive indicators distinguishing successful from failed trials; this question, however, has not yet been examined within a single forehand-drive task.

This study used amateur players as participants, partly because the amateur population shows more substantial variability in stroke stability, making the contrast between successful and failed trials more informative for observation, and partly because this restricts the conclusions mainly to amateur and training populations, so that extrapolation to elite players requires caution. On this basis, the present study systematically compared the support-base mechanical features of successful and failed trials within the same standardised forehand-drive task. Force-plate-derived summed bilateral GRF components and combined COP indicators served as the primary analysis targets, examining force magnitude (mean, peak, impulse), movement-onset-referenced and relative timing of force peaks, and the movement speed, path length and mediolateral fluctuation of the COP; because force-timing indicators depend on the definition of the movement window for a single stroke, the total movement duration was also examined so that the peak-timing results could be interpreted directly rather than only by inference. In addition, the robustness of the trial-level primary results was tested by excluding participants who contributed successful trials only, by body-weight-normalised GRF sensitivity analysis and by contact-related time-window analysis. Several discrete kinematic indicators extracted by markerless motion capture (e.g. key joint angles) were used only as auxiliary interpretation; because markerless systems still have accuracy limits during high-speed swings and limb occlusion, the kinematic results were positioned as exploratory evidence, whereas the principal conclusions were built on force-plate data that are independent of motion capture, ensuring that the core findings are not affected by kinematic estimation error.

Accordingly, the following hypotheses were proposed: compared with successful trials, failed trials would show reduced support-base control, that is, greater COP movement speed, path length and mediolateral fluctuation, together with altered force-peak timing; whereas for force magnitude, this study did not presuppose that failure arises from “insufficient force”, but treated its direction as an open question, to examine whether the common intuition that “a failed stroke equals insufficient force production or racket speed” holds.

Methods

Participants

Fourteen amateur table-tennis players served as participants (10 men, 4 women; age 20.9 ± 2.0 years; height 173.2 ± 4.3 cm). Body mass data were available for 13 participants (64.6 ± 5.6 kg). All participants were of amateur level without athletic grading and reported no lower-limb injury within the previous six months that affected training or testing. Participants took part voluntarily and signed written informed consent; the study was approved by the Ethics Committee of the authors' institution and complied with the Declaration of Helsinki.

Experimental design and protocol

A within-participant design was adopted, taking successful and failed trials performed by the same player within the same standardised forehand-drive task as the units of comparison, thereby controlling between-individual confounders such as performance level, anthropometric characteristics and individual motor-control strategy, so that between-outcome differences could be examined more directly as mechanical features associated with stroke outcome [19]. A table-tennis serving machine (Oukei, model TW-2700-ES9, Guangdong, China) delivered topspin balls to the serving area. The machine parameters were set uniformly as follows: ball-feed frequency 70 balls/min (i.e. one ball every 0.86 s); nominal ball speed approximately 7 m/s (based on the machine setting, not independently re-measured with a separate speed-measuring device); landing-position setting 2; upper-wheel speed/spin setting 3.8 and lower-wheel speed/spin setting 2.0. Balls landed in the participant's forehand serving area, with a landing zone of approximately 65 cm × 40 cm (length × width); the centre of the landing zone was approximately 69.5 cm from the net and 67.5 cm from the end line, and the machine body was approximately 0.40 m from the table end line. Participants were required to return the ball with a forehand drive to the opposite half of the table and, as far as possible, into a pre-marked target area (approximately 135 cm × 75 cm, length × width; the inner sideline approximately 2 cm from the net and the outer sideline against the end line) so as to standardise stroke direction. Before formal testing, each participant performed 10 familiarisation strokes to become accustomed to the ball rhythm. Trials were classified by whether the return produced a legal landing: a ball that crossed the net and landed within the opposite half-table (not necessarily within the target area) was classified as a successful trial (successful return), whereas a ball that went into the net or out of bounds (failing to cross the net or landing beyond the table surface) was classified as a failed trial (stroke error). The reason for dichotomising by legal landing rather than by within-table landing accuracy is that net and out-of-bounds errors are the most clearly and objectively determinable forms of error in a competitive context. The experimental layout and the striking area are shown in Fig. 1.

Kinematic data were acquired with a markerless motion-capture system (FASTMOVE V1.0, Dalian Ruidong Technology, Liaoning, China) comprising 4 cameras, at a capture frame rate of 50 frames/s, with cameras mounted at a height of 3.0–3.5 m and inter-camera angles of 60°–120°. Before testing, the capture volume was calibrated with an "L"-shaped coordinate frame and a "T"-shaped wand; the standard deviation of the wand length for all 4 cameras was below 0.8 mm, and cameras exceeding the calibration threshold were environmentally shielded to meet capture requirements. All devices were triggered uniformly by the FASTMOVE capture software; after capture, landmarks were named within the software, and incomplete trajectories were filled by linear or polynomial interpolation. The validity of automatic landmark identification by this type of markerless motion-capture system has been supported by previous research: the automatically identified three-dimensional landmark coordinates were highly consistent with manual digitization (for most landmarks the multiple correlation coefficient exceeded 0.95 and the discrepancy was below 0.015 m) [22].

Concurrently with kinematic acquisition, lower-limb kinetic data were acquired by 2 three-dimensional force plates (FP6050-FM, Kunwei Technology, Jiangsu, China) at a sampling frequency of 1000 Hz. The motion-capture and force-plate systems were synchronised using a shared hardware trigger/TTL pulse, and temporal alignment was verified during preprocessing. Each force plate was equipped with 4 piezoresistive three-dimensional force sensors, with a plate surface of 600 mm × 500 mm, measurement ranges of 2500 N for the anteroposterior (Fx) and mediolateral (Fy) directions and 5000 N for the vertical (Fz) direction, overload capacities of 7500 N and 15000 N respectively, accuracy of 0.5% FS, linearity and hysteresis both ± 0.3% FS, channel crosstalk 0.5% FS, sampling resolution 24 bit, and natural frequencies of 300 Hz horizontally and 200 Hz vertically. The participant's two feet were placed on the 2 force plates separately, with plate 1 and plate 2 recording the right and left foot

respectively. The force plates were operated according to the manufacturer's specifications and were calibrated before data collection.

Given the accuracy limits of markerless motion capture during high-speed swings and limb occlusion [23–25], the analysis was divided into two tiers: force-plate-derived summed bilateral GRF components and combined COP indicators, acquired directly by the force plates and independent of motion capture, constituted the primary analysis, whereas the markerless kinematic indicators constituted an exploratory auxiliary analysis used only for directional interpretation.

Trial inclusion and exclusion criteria were as follows: trials with missing landmarks, abnormal force signals or incomplete data were excluded. The exploratory kinematic analysis and the primary kinetic analysis were based on two mutually independent, non-nested datasets, each with its own inclusion criteria. The kinetic analysis required both feet to remain fully on their respective force plates at the instant of ball contact and the force signals to be free of artefacts, a relatively strict criterion; the 14 participants contributed on average about 13.5 valid trials each (189 in total; of which 140 were legal returns and 49 were stroke errors). The kinematic analysis required only a stable three-dimensional landmark reconstruction for a given stroke; of the participants, 6 were excluded in their entirety because of limb occlusion or trajectory loss that prevented reconstruction, whereas for the remaining 8 participants any stroke with a successful reconstruction was included, without the force-plate landing constraint, yielding on average about 26.4 observations each (211 in total). The kinematic sample therefore had fewer participants but more observations: the number of participants depended on the success rate of three-dimensional reconstruction, whereas the number of observations per participant depended on each participant's inclusion criterion, the two varying along different dimensions.

Indicator extraction and computation

The raw three-dimensional force signals were first low-pass filtered with a fourth-order zero-phase Butterworth filter (cut-off frequency 50 Hz) to remove high-frequency noise, after which the following indicators were extracted. GRF magnitude indicators and combined COP indicators were the primary outcomes, and force-peak timing was a secondary outcome. Both plates recorded three-dimensional force. The prespecified kinetic indicators were the mean, peak, impulse, time to peak from movement onset and relative time to peak of the summed bilateral anteroposterior (Fx = Fx1 + Fx2), mediolateral (Fy = Fy1 + Fy2) and vertical (Fz = Fz1 + Fz2) GRF components, together with the plate-2 left-foot vertical component (Fz2). No plate-specific Fx1/Fx2 or Fy1/Fy2 outcomes were included in the reported 30-indicator family. Impulse was the integral of the force–time curve over the movement window (Eq. 1); the relative time to peak was the time to peak from movement onset expressed as a percentage of the movement duration (Eq. 2).

This study followed the coordinate definitions output by the laboratory acquisition system and the force plates: Fx, Fy and Fz denote the summed bilateral anteroposterior, mediolateral and vertical ground reaction forces, respectively, and Fz2 denotes the left-foot vertical ground reaction force recorded by plate 2. Because the sign of the horizontal force components may be affected by the laboratory coordinate system, stance and stroke direction, this paper mainly interprets between-outcome differences in the GRF indicators of each direction within the same coordinate system, and does not make mechanical attributions of the horizontal forces to specific push, pull, or medial/lateral directions beyond the scope of the data definition.

$$J = \int_{[t0,\,t1]} F(t)\,dt \quad (1)$$

$$\mathrm{RelTime} = [(t_{peak} - t0) / (t1 - t0)] \times 100\% \quad (2)$$

Here t_0 and t_1 are the start and end instants of the analysed movement interval for a single forehand drive, identified from near-zero or local-minimum events in the resultant racket-speed curve according to the predefined event-detection procedure: t_0 was the start of movement from a near-rest state, and t_1 was the post-follow-through return to a near-rest state. This start–end definition was the operational segmentation criterion of this study and was verified by trial-by-trial visual quality control; a MediaPipe-based framework for quantifying table-tennis forehand strokes indicates that automated kinematic quantification is methodologically feasible for this task [26], but the start/end points and contact-related windows in this study remain operational event definitions. Because the movement start and end points were defined from a 50 frames/s markerless

kinematic signal, event localisation has an uncertainty of approximately one video frame (20 ms), and results involving absolute timing are interpreted only with caution, and core conclusions were based preferentially on GRF and COP indicators for which contact-window sensitivity analyses were conducted, rather than on absolute timing indicators alone. The instant of ball contact (ball–racket contact) was identified separately as an independent event within this interval [27]. The raw timestamp of each force peak was first identified in the force-plate time base; the reported Time_to_peak_from_start variable was then computed as t_peak − t_0 and expressed in milliseconds. The denominator (t_1 − t_0) of RelTime_at_Max was the total duration of the movement interval, used to express the same peak time in relative terms [28].

The COP indicators were the sway path length, mean speed, mediolateral root mean square (RMS_ML), the anteroposterior and mediolateral COP ranges (Range_AP, Range_ML) and the mean anteroposterior COP position (Mean_AP) of the combined centre of pressure of the two feet (COPcomb). The combined COP was obtained by weighting the COP positions of the two plates by their respective vertical forces (Eq. 3, where r1 and r2 are the COP positions of the two plates); the sway path length was the sum of displacements between adjacent samples (Eq. 4, where N is the number of samples); the mean speed was the ratio of path length to movement duration (v = L / T); the mediolateral RMS reflected the magnitude of mediolateral fluctuation (Eq. 5); the anteroposterior and mediolateral COP ranges (Range_AP, Range_ML) were the maximum-minus-minimum COP displacement within the movement window; and the mean anteroposterior COP position (Mean_AP) was the arithmetic mean of the anteroposterior COP coordinate over the same window, interpreted only as a within-system positional descriptor because it depends on the laboratory coordinate system [29, 30].

$$COP(t) = [Fz1(t) \times r1(t) + Fz2(t) \times r2(t)] / [Fz1(t) + Fz2(t)] \quad (3)$$

$$L = \Sigma[i = 1 \text{ to } N - 1] \sqrt{[(x(i + 1) - x(i))^2 + (y(i + 1) - y(i))^2]} \quad (4)$$

$$RMS_ML = \sqrt{[(1/N) \Sigma[i = 1 \text{ to } N] (xi - xbar)^2]} \quad (5)$$

Support-base mechanical loading has been used to characterise lower-limb loading in sport-specific table-tennis movements [31], supporting the use of GRF and COP as primary analysis indicators. The exploratory kinematic indicators included the major joint angles (shoulder, hip, knee), trunk rotation angle and centre-of-mass (COM) position; proxy-model-based joint moments/powers were not included because of the absence of complete musculoskeletal-modelling quality control (scaling, inverse-dynamics verification [32, 33]).

The exploratory kinematic indicators were computed from the three-dimensional landmark coordinates output by the markerless motion-capture system using a Python-based workflow (relying on open-source libraries such as ezc3d, NumPy, SciPy and pandas), the main steps being: (1) a fourth-order zero-phase Butterworth low-pass filter (cut-off frequency 10 Hz) was applied to each landmark trajectory to suppress high-frequency noise; (2) each joint centre was determined from the geometric centre of the corresponding surface landmarks, with the hip-joint centre estimated by the regression method of Bell et al.; because direct pelvic-width landmarks were unavailable, the pelvic-width input was inferred from shoulder width through a study-specific exploratory anthropometric approximation informed by de Leva's segmental anthropometric data [34, 35]; (3) each joint angle was computed as the angle between adjacent segment vectors within the corresponding anatomical plane, following clinical sign conventions; (4) the whole-body centre of mass (COM) was obtained by the segmental method, weighted by de Leva's segmental mass ratios and centre-of-mass positions [35]; and (5) each trial was time-normalised to 0–100% of the movement duration (101 points, cubic-spline interpolation), and the within-participant repeatability across trials was characterised by the across-trial standard deviation and root mean square (RMSE) of the time-normalised curves of each participant. Bell's regression method and de Leva's segmental parameters are published biomechanical methods [34, 35], but the shoulder-to-pelvis approximation used here is not itself a validated standard method and should be regarded as exploratory. This study did not conduct an independent concurrent-validity test of the joint-centre, joint-angle or centre-of-mass workflow against gold standards such as marker-based motion capture or musculoskeletal modelling. The validity of the downstream kinematic quantities is therefore only indirectly supported by the cited methodological basis and within-participant repeatability, rather than directly verified. For this reason, the kinematic results are used only as exploratory, directional evidence, and all core conclusions are built on three-dimensional force-plate data that are independent of motion capture.

Statistical analysis

For each indicator, a linear mixed model (LMM) was fitted separately, with stroke outcome as a fixed effect and participant code as a random intercept (Eq. 6, where G is stroke outcome and u_i is the participant random effect), to handle the within-participant correlation of multiple trials from the same participant and the imbalance in trial numbers between participants [36]; the models were implemented in the linear-mixed-model module of JASP (0.97.0) [37], fitted on the basis of lme4 [38], with parameters estimated by restricted maximum likelihood (REML), fixed-effect significance judged by Type III sum-of-squares F tests, and denominator degrees of freedom approximated by the Satterthwaite method [36, 39].

$$Yij = \beta 0 + \beta 1Gij + ui + \varepsilon ij,\ ui \sim N(0, \sigma u^2) \quad (6)$$

The fixed-effect P values of the 30 GRF/COP indicators were corrected for the false discovery rate (FDR) by the Benjamini-Hochberg method: the P values were sorted in ascending order and judged significant at and below the largest rank k satisfying Eq. 7 (m = 30, q = 0.05) [40]; between-outcome differences were reported as the difference in estimated marginal means (EMM) and its 95% confidence interval (CI), the estimated marginal means being obtained with the estimated-marginal-means procedure in JASP 0.97.0 [37], following the least-squares-means framework implemented in the emmeans package [41]. Exploratory markerless posture-kinematic indicators were analysed separately using trial-level mixed-effects models with stroke outcome as a fixed effect and participant code as a random intercept. This exploratory kinematic analysis included 211 trial-level observations from eight participant codes. Proxy racket-speed variables derived from distal/finger landmarks were retained only for audit and were excluded from the reported posture-kinematic FDR family. Benjamini-Hochberg FDR correction was applied across the nine reported posture-kinematic indicators, and only $q < 0.05$ results were treated as hypothesis-generating auxiliary findings.

$$P(k) \le (k/m)q \quad (7)$$

On this basis, two model-derived effect-size summaries were reported. Partial η^2 (partial eta squared) was calculated from the F value and degrees of freedom (Eq. 8) and is reported as an F-statistic-derived effect-size estimate rather than as a direct proportion of outcome variance explained. A model-based standardised mean difference (SMD) was calculated as the absolute difference in estimated marginal means between failed and successful trials divided by the square root of the sum of the random-intercept variance and residual variance (Eq. 9). This quantity is not the paired-sample Cohen's dz. For descriptive context only, SMD values were compared with conventional 0.2/0.5/0.8 benchmarks and partial-η^2 values with 0.01/0.06/0.14 benchmarks [42]; these thresholds were not used for statistical inference.

$$\eta p^2 = (F \times df1) / (F \times df1 + df2) \quad (8)$$

$$SMD = |Mfailed - Msuccessful| / \sqrt{(\sigma u^2 + \sigma e^2)} \quad (9)$$

All 30 linear mixed models included in the diagnostics completed REML estimation without convergence failure; for boundary models in which the random-intercept variance approached 0, the results were retained and flagged in the residual diagnostics, but were not used alone as a basis for conclusions. Model-assumption checks included variable-distribution inspection (mean, standard deviation, median, interquartile range, skewness, kurtosis and standardised outliers) and residual diagnostics (residual-versus-fitted plots, residual Q–Q plots, standardised residuals, the Shapiro–Wilk normality test, the Spearman correlation between the absolute residuals and the fitted values, and the Levene test of homogeneity of variance grouped by stroke outcome); given that, at this sample size (189), the Shapiro–Wilk test is sensitive to slight departures from normality, the diagnostics did not rely on its P value alone but were assessed comprehensively together with the Q–Q plots, standardised outliers and heteroscedasticity checks.

To further assess whether the trial-level LMM results were affected by unequal participant contribution or body-mass scale, several sensitivity analyses were added. First, the 2 participants who contributed successful trials only and no failed trials were excluded, and only the 12 participants who had both successful and failed trials were retained, with the primary LMMs of the 30 GRF/COP indicators refitted.

In addition, to assess whether the GRF differences in raw newton values might be driven by body-mass scale, a body-weight-normalised GRF sensitivity analysis was conducted. This analysis used the registered body mass from the participant information sheet to compute body-weight force (body mass in kg × 9.80665). Because P12's registered body mass was missing and P12 contributed successful trials only, the main body-weight-normalised sensitivity analysis was performed on the 12-participant-code sample after excluding P09 and P12; this sample comprised 169 trials (120 successful, 49 failed), and all included codes had a registered body mass. GRF means and peaks divided by body-weight force were expressed in BW, and GRF impulses divided by body-weight force were expressed in BW·s. The COP indicators, Time_to_peak_from_start and RelTime_at_Max were not body-weight-normalised. Each normalised GRF indicator was analysed with an LMM consistent with the primary analysis, and the P values of the 12 normalised GRF magnitude/impulse indicators were FDR-corrected by the Benjamini-Hochberg method.

To test whether the GRF/COP differences within the full movement window might be affected by post-contact follow-through or compensatory actions, a contact-related-window sensitivity analysis was further conducted on the basis of the trial-by-trial calibrated ball–racket contact frame. The contact-frame table was matched to the original 189 kinetic trials by participant, stroke outcome and within-group trial order, and all original trials were successfully matched. An additional P09 failed trial that appeared in the contact-frame table did not belong to the original 189-trial analysis dataset and was therefore not included. One P07 successful trial had an ordering error in which the contact frame was later than the movement-end frame, and was therefore used only for the full marked window and not for the contact-related windows. Five window indicators were re-extracted from the raw C3D force-plate data: the full marked window, start-to-contact, from 300 ms before contact to contact, from 200 ms before contact to contact, and from 200 ms before contact to 50 ms after contact. For each window, component-specific time to peak was calculated as the force-peak time minus that window's start and expressed in milliseconds; absolute acquisition timestamps were not analysed as time-to-peak outcomes. For each window, an LMM was fitted with the same model form as the primary analysis, and BH-FDR correction was applied across the complete family of 30 indicators within that window.

Given that the sex ratio of the sample was not fully balanced and that sex is a participant-level variable, this study did not treat sex as a primary explanatory factor and did not perform sex-stratified inference; to assess the potential influence of the sex composition on the principal results, a sex-adjusted sensitivity model was built on the basis of the primary model, adding sex to the fixed effects and retaining the participant-code random intercept. Because the number of female codes was limited, a "stroke outcome × sex" interaction term was not included and the sex main effect was not interpreted; this analysis was used only to determine whether the stroke-outcome effect remained stable in direction and magnitude after sex adjustment.

No a priori sample-size calculation was performed; the sample size was determined by the number of participants and the valid kinetic trials available after quality control. The statistical results should therefore be interpreted as exploratory and require confirmation in larger, adequately powered samples.

Results

Primary analysis of support-base kinetics and COP indicators

After FDR correction, 15 of the 30 prespecified GRF/COP indicators differed significantly between successful and failed trials ($q < 0.05$; Table 1, Figs. 2 and 3; Additional file 1: Table S2). The timing results no longer supported a shared three-component absolute peak-timing feature; instead, failed trials showed a later anteroposterior time to peak from movement onset and a later relative anteroposterior peak time (Table 1, Fig. 2). With respect to the open question of force magnitude, the results were contrary to the intuition that "failure arises from insufficient force": the summed bilateral anteroposterior force (mean, peak, impulse), summed bilateral vertical force (mean, peak) and left-foot vertical force (mean, peak) of the failed trials were all significantly higher than those of the successful trials (Fig. 3).

The sex-adjusted sensitivity analysis showed that the principal results were robust (Additional file 1: Table S7): at the trial level there were 60 female and 129 male trials, and at the participant-code level 4 female and 10 male codes, with failure rates of

33.3% (20/60) for female trials and 22.5% (29/129) for male trials; all 30 sex-adjusted models converged, the direction of the failed–successful effect and the judgement of whether the confidence interval crossed 0 were unchanged after adding sex, and 15/30 indicators remained FDR-significant after sex adjustment. The largest relative estimate change was 23.4% for the non-significant Fz2 time-to-peak variable; the other indicators showed smaller changes, indicating that the principal differences were insensitive to sex adjustment.

Table 1
Linear-mixed-model results for differences in kinetic and COP indicators between successful and failed trials.

Indicator (unit)	Failed	Success	Δ (F − S)	95% CI	F	P	q	η²□	Model-based SMD
Mean anteroposterior force Mean(Fx)/N	32.55	27.32	5.24	2.53 to 7.94	14.60	< .001	< .001	0.077	0.37
Peak anteroposterior force Max(Fx)/N	59.95	51.73	8.22	4.42 to 12.02	18.20	< .001	< .001	0.094	0.38
Anteroposterior impulse Impulse(Fx)/(N·s)	11.19	9.94	1.24	0.27 to 2.21	6.38	0.012	0.027	0.035	0.26
Fx time to peak from onset Time_to_peak_from_start(Fx)/ms	177.05	122.11	54.93	22.00 to 87.87	10.84	0.001	0.005	0.058	0.40
Relative time to peak of anteroposterior force RelTime_at_Max(Fx)/%	48.74	32.84	15.90	7.35 to 24.46	13.45	< .001	0.001	0.071	0.45
Mean combined vertical force Mean(Fz)/N	642.01	613.56	28.45	14.47 to 42.44	16.12	< .001	< .001	0.085	0.27
Peak combined vertical force Max(Fz)/N	849.59	817.40	32.19	5.14 to 59.24	5.51	0.020	0.040	0.031	0.13
Mean left-foot vertical force (plate 2) Mean(Fz2)/N	328.75	307.68	21.07	10.26 to 31.88	14.79	< .001	< .001	0.078	0.29
Peak left-foot vertical force (plate 2) Max(Fz2)/N	471.20	425.49	45.71	27.31 to 64.10	24.04	< .001	< .001	0.121	0.40
COP mean speed MeanSpeed(COPcomb)/(mm·s⁻¹)	235.28	190.11	45.17	16.28 to 74.05	9.53	0.002	0.007	0.052	0.31
COP sway path length SwayPathLength(COPcomb)/mm	86.13	68.73	17.40	6.52 to 28.28	9.96	0.002	0.006	0.054	0.31
COP ML RMS RMS_ML(COPcomb)/mm	8.98	6.58	2.40	0.64 to 4.16	7.27	0.008	0.021	0.039	0.39
COP AP range Range_AP(COPcomb)/mm	40.69	32.51	8.18	1.96 to 14.41	6.74	0.010	0.024	0.037	0.25
COP ML range Range_ML(COPcomb)/mm	28.53	21.87	6.67	1.59 to 11.74	6.73	0.010	0.024	0.037	0.36

Note: EMM, estimated marginal mean; 95% CI, 95% confidence interval of the difference; F and P, the fixed-effect test statistic of the LMM and corresponding P value; q, the Benjamini-Hochberg-corrected P value; partial η², an F-statistic-derived effect-size estimate (Eq. 8); model-based SMD, the absolute difference in EMM between failed and successful trials divided by the square root of the sum of the random-intercept variance and residual variance (Eq. 9). The model-based SMD is not paired-sample Cohen's dz. Fx, Fy and Fz are the summed bilateral anteroposterior, mediolateral and vertical ground reaction forces; Fz2 is the left-foot vertical force recorded by plate 2; and COPcomb is the combined centre of pressure of the two feet. Time_to_peak_from_start is the time from movement onset (t0) to the force peak, expressed in ms; RelTime_at_Max is the same peak time normalised to movement duration. SMD values are presented as absolute standardised mean differences.

Indicator (unit)	Failed	Success	Δ (F − S)	95% CI	F	P	q	η²□	Model-based SMD
COP mean AP Mean_AP(COPcomb)/mm	67.57	79.83	−12.26	−17.84 to −6.69	18.84	< .001	< .001	0.098	0.13

Note: EMM, estimated marginal mean; 95% CI, 95% confidence interval of the difference; F and P, the fixed-effect test statistic of the LMM and corresponding P value; q, the Benjamini-Hochberg-corrected P value; partial η², an F-statistic-derived effect-size estimate (Eq. 8); model-based SMD, the absolute difference in EMM between failed and successful trials divided by the square root of the sum of the random-intercept variance and residual variance (Eq. 9). The model-based SMD is not paired-sample Cohen's dz. Fx, Fy and Fz are the summed bilateral anteroposterior, mediolateral and vertical ground reaction forces; Fz2 is the left-foot vertical force recorded by plate 2; and COPcomb is the combined centre of pressure of the two feet. Time_to_peak_from_start is the time from movement onset (t0) to the force peak, expressed in ms; RelTime_at_Max is the same peak time normalised to movement duration. SMD values are presented as absolute standardised mean differences.

Altered force-peak timing in failed trials

As a secondary result, the corrected force-peak timing indicated a later anteroposterior support-force peak in failed trials, both in absolute time from movement onset and in relative movement phase (Table 1, Fig. 2). This timing result was specific to Fx; Fy, Fz and Fz2 timing indicators did not survive FDR correction and were therefore not interpreted as a shared global peak-timing feature.

Increased COP movement and mediolateral fluctuation in failed trials

The combined-COP mean speed, sway path length and mediolateral RMS of the failed trials were all higher than those of the successful trials, indicating greater support-point movement and mediolateral fluctuation (Table 1, Fig. 2).

Exploratory kinematic results

The exploratory kinematic analysis included 211 trial-level observations (8 participant codes) and was positioned as an auxiliary analysis. After FDR correction, the right shoulder elevation angle and the left knee flexion angle at ball contact reached $q < 0.05$, both being lower in failed trials (Table 2, Fig. 4; Additional file 1: Table S5). The combined-vertical-force phase curve showed that failed trials were higher in the early phase of the movement and had a different maintenance pattern in the later phase (Fig. 5). Because the results derived from 50 frames/s markerless motion capture, and because the kinematic analysis and the primary kinetic analysis were based on non-nested datasets, the kinematic results serve only as supplementary evidence.

Table 2
FDR-significant exploratory kinematic indicators.

Indicator (unit)	Failed mean	Successful mean	Observed Difference (failed − successful)	P	q_FDR	Significance
Right shoulder elevation angle at contact hit_R_shoulder_elev/(°)	160.44	163.18	−2.73	0.003	0.018	*
Left knee flexion angle at contact hit_L_knee_flexion/(°)	147.25	149.16	−1.91	0.004	0.018	*

Note: this table presents the indicators at $q < 0.05$ after FDR correction in the kinematic auxiliary (exploratory, hypothesis-generating) analysis; these FDR-significant exploratory kinematic indicators are also summarised in Additional file 1: Table S5. Owing to the processing limits of the kinematic data, the strength of interpretation is lower than that of the kinetic/COP primary analysis; this analysis included 211 trial-level observations in total. Failed and successful means and the displayed difference are observed group means; P values and q values are from trial-level mixed-effects models.

Participant trial contribution and exclusion sensitivity analysis

To assess whether the trial-level comparison was affected by unequal participant contribution, the numbers of successful and failed trials contributed by each participant were tabulated (Additional file 1: Table S1). The 14 participants contributed 189 kinetic trials in total (140 successful, 49 failed), with an overall failure rate of 25.9%; 12 participants contributed at least 1 failed trial, and 2 participants contributed successful trials only. After excluding P09 and P12, who contributed successful trials only, the sensitivity sample comprised 12 participants and 169 trials (120 successful, 49 failed). After refitting the LMMs of the 30 GRF/COP indicators, the failed-successful direction of the core GRF/COP indicators was consistent with that of the full sample, indicating that the principal results did not depend on the participants who contributed successful trials only.

Contact-related-window sensitivity analysis

The contact-frame-window sensitivity analysis further showed that the direction of the effects in the contact-related windows was generally stable (Additional file 1: Tables S3 and S6). The full marked window comprised 169 trials after excluding P09 and P12; the contact-related windows comprised 168 trials because of the contact-frame ordering error in one P07 successful trial. Supplementary Table S3 summarises the 15 indicators that were FDR-significant in the primary full-sample analysis, whereas Supplementary Table S6 reports all 30 indicators; in both tables, BH q values were calculated across the complete 30-indicator family separately within each window. All 15 Table 1 indicators retained the direction of their full marked-window estimates in each contact-related window. After FDR correction, 8 indicators remained significant in the 300 ms-before-contact-to-contact window, 3 in the 200 ms-before-contact-to-contact window, 6 in the 200 ms-before-contact-to-50 ms-after-contact window, and 1 in the start-to-contact window. In the shorter windows, the effects of some force-magnitude and impulse indicators were reduced, indicating that the full-window results were not entirely driven by post-contact follow-through but that some effects were sensitive to window length.

Body-weight-normalised GRF sensitivity analysis

The body-weight-normalised sensitivity analysis was performed on the 12-participant-code sample after excluding P09 and P12; among the included participant codes, registered body mass was 64.0 ± 7.2 kg (mean ± SD). After body-weight normalisation, the failed-successful differences of all 12 GRF magnitude/impulse indicators were positive, indicating that the direction in every case was higher in failed than in successful trials. Of these, 7/12 indicators remained significant after FDR correction, namely Mean_Fx_BW, Max_Fx_BW, Impulse_Fx_BWs, Mean_Fz_BW, Max_Fz_BW, Mean_Fz2_BW and Max_Fz2_BW (Additional file 1: Table S4). In a full-sample reference analysis, after recovering body mass using the 13 registered body masses and the C3D weight event for P12, the direction of all 12 indicators was likewise failed > successful, with 7/12 indicators FDR-significant. Therefore, the core conclusion of the primary analysis that “failed trials have higher GRF” is unlikely to be driven by between-participant body-mass differences alone.

Discussion

This study compared successful and failed forehand drives within the same standardised task and found that failed trials were mainly accompanied by higher anteroposterior and vertical ground reaction forces and by greater COP mean speed, path length and mediolateral fluctuation; the force-peak timing was also altered, but because it is affected by the definition of the movement window and by temporal resolution, it is interpreted here with caution as a secondary result. The added sensitivity analyses showed that the direction of the core effects was generally consistent across exclusion of participants who contributed successful trials only, body-weight-normalised GRF models and multiple contact-related windows, although some short-window effect sizes were reduced. The most robust conclusion of this study is therefore that a stroke error does not correspond to reduced support-base force output but rather to higher support-base loading and greater COP excursion within the present amateur forehand-drive task.

The higher support-base mechanical quantities in failed trials may reflect excessive support-base force production, a mismatch between support and swing rhythm, or increased postural adjustment before and after the stroke, rather than insufficient force reserve. The within-participant design and the standardised ball feeding from the serving machine controlled part of the between-individual differences and of the incoming-ball difficulty; the higher force together with greater COP movement and

altered peak timing formed a coherent picture of “imbalanced force organisation” rather than “insufficient force”; and the exploratory kinematic results also suggested that some postural indicators at ball contact may have been lower in failed trials. However, because this study was an observational trial-level comparison and the full movement window included the pre-stroke preparation, ball–racket contact and follow-through phases, the above pattern should not be interpreted as strict causal evidence. This is consistent with the view that performance in racket sports depends on the matching of speed, timing and kinetic-chain transfer rather than on force peaks alone [21].

The most important robustness evidence of this study is not that all sensitivity analyses retained exactly the same significance, but that the direction of the core effects was consistent across exclusion of participants who contributed successful trials only, body-weight normalisation and contact-related time windows. After excluding participants who contributed successful trials only, the direction of the trial-level LMM results remained stable, and the body-weight-normalised GRF analysis further indicated that the principal anteroposterior and vertical force-magnitude differences were not simply caused by body-mass scale. In shorter contact-related windows, some FDR-significant effects were reduced, indicating that part of the full-window result was sensitive to window length and should not be read as a causal or training-prescriptive result.

The contact-frame-window analysis also provided a boundary for interpreting the full-window results. If the GRF/COP differences were produced entirely by emergency adjustments after the stroke or by follow-through compensation, the direction should weaken markedly or even reverse in the pre-contact or near-contact windows. However, this study observed consistent direction of the core indicators in the start-to-contact, 300 ms-before-contact-to-contact, 200 ms-before-contact-to-contact, and 200 ms-before-contact-to-50 ms-after-contact windows, indicating that these differences were not driven solely by post-contact compensatory actions. On the other hand, the effect sizes and FDR significance of some force-magnitude and impulse indicators decreased in the shorter windows, indicating that some of the full-window differences may include the combined contributions of pre-stroke preparation, support regulation at the instant of contact, and post-stroke follow-through/postural adjustment. A more cautious interpretation is therefore that failed trials are accompanied by systematic differences in support-base mechanical organisation and COP control around contact, rather than that all differences occur before the stroke and directly cause failure.

The body-weight-normalised GRF sensitivity analysis further addressed the question of whether the raw-newton mechanical indicators might be affected by body-mass differences. After normalisation, failed trials were still higher than successful trials in the principal anteroposterior and vertical GRF magnitude indicators, and most core force-magnitude indicators remained significant after FDR correction, indicating that the conclusion of the primary analysis that “failed trials have higher GRF” is unlikely to be explained solely by heavier participants contributing more failed trials. At the same time, the statistical evidence for the mediolateral force and some impulse indicators weakened after normalisation, indicating that the interpretation should not be extended to claim that all directions and all impulse indicators are equally robust; a more cautious statement should focus on the anteroposterior and vertical GRF magnitudes and the COP-movement-related indicators.

The corrected force-peak timing result was more limited than in the earlier absolute-timestamp analysis. Failed trials showed a later anteroposterior force peak from movement onset (177.0 vs 122.1 ms; failed − successful = 54.9 ms, 95% CI 22.0 to 87.9 ms) and a later relative anteroposterior peak phase (48.7% vs 32.8%), whereas Fy/Fz/Fz2 timing indicators did not survive FDR correction. Therefore, the timing result should be interpreted as an Fx-specific delay in support-force organisation rather than as a shared global force-peak event. Movement duration was shorter on average in failed trials (failed − successful = − 11.2 ms, 95% CI − 25.0 to 2.5 ms), but this difference was not statistically significant; given the 50 frames/s movement-window definition, timing findings remain secondary.

The COP indicators provided evidence at the level of balance regulation that is compatible with the GRF results. The higher combined-COP speed, path length and mediolateral fluctuation in failed trials directly reflect greater support-point movement and mediolateral fluctuation; the combined COP of the two feet characterises overall support control better than unilateral indicators. Although these COP indicators suggest increased support-control fluctuation, they cannot by themselves be equated with a directly measured decrease in overall postural stability. The greater COP movement is consistent with evidence that different foot-contact patterns alter lower-limb mechanics [13], and support-control fluctuation may relate simultaneously to performance and to lower-limb loading, with its potential significance for injury risk awaiting dedicated research [17].

The exploratory kinematic results were directionally compatible with the principal results: the right shoulder elevation angle and the left knee flexion angle at ball contact were lower in failed trials, suggesting that the support–posture matching may differ from that of successful trials. However, because this result derived from markerless motion capture, which has systematic error [23, 24], and because the kinematic analysis and the primary kinetic analysis were based on non-nested datasets, it is used only as a supplementary interpretation; the core conclusions remain based on the force-plate data, which are independent of it.

At the practical level, the technical evaluation of the forehand drive should not take force magnitude or movement amplitude as the sole criterion. In this study, failure was in fact accompanied by greater support force, COP movement and mediolateral fluctuation, suggesting that single-mindedly pursuing “greater force” may be counterproductive; the matching among stable lower-limb support, coordinated push-and-rotation, stroke timing and follow-through control may be more conducive to improving the success rate than simply increasing force. At present, the GRF and COP indicators can serve only as candidate objective indicators for assessing the support-base organisation state of the forehand drive, and their diagnostic value for training still needs to be verified by longitudinal or interventional studies.

This study still has several limitations. First, the participants were 14 amateur players, the sample was small and the sex ratio unbalanced, so the results apply mainly to the amateur forehand-drive task under standardised, well-prepared conditions, and extrapolation to elite players or competitive situations requires caution. Second, although the within-participant design and the standardised ball feeding from the serving machine controlled part of the confounding, the incoming-ball difficulty was not necessarily fully balanced between successful and failed trials, and the higher mechanical quantities of failed trials may partly stem from differences in incoming-ball difficulty; because the incoming-ball difficulty was not independently quantified on a trial-by-trial basis (the nominal ball speed was the machine setting and was not measured for each ball), and because trials were grouped by outcome, this confounder cannot be completely excluded, although the high directional consistency across the core indicators is difficult to explain by a single incoming-ball perturbation alone. Third, although the primary analysis used an LMM to handle the within-participant correlation of repeated trials, the models included participant random intercepts only and did not model participant-specific stroke-outcome slopes; if outcome effects vary materially between participants, this specification may underestimate uncertainty. The truly independent unit of information is still limited by the number of participants, so confirmation in a larger participant sample is required. Fourth, the distribution of failed trials across participants was not fully balanced, with 2 participants contributing no failed trials; the trial-level sensitivity analysis after excluding these 2 participants showed stable direction, but the uncertainty due to the small sample and the imbalanced trials cannot be completely eliminated. Fifth, in the body-weight-normalised sensitivity analysis the registered body mass of P12 was missing, so the main analysis used the 12-participant registered-body-mass sample after excluding P09 and P12; although the direction and significance of the principal GRF magnitude indicators remained stable, the statistical evidence for the Fy direction and some impulse indicators weakened. Sixth, the full movement window contained the pre-stroke preparation, ball–racket contact and post-stroke follow-through components and may have included some post-contact compensatory actions; the contact-frame-window sensitivity analysis showed that the direction of the core effects was consistent in the contact-related windows, but some effect sizes and significance decreased in the shorter windows, so not all GRF/COP differences can be interpreted as a strict pre-stroke causal mechanism. Seventh, the exploratory markerless kinematic analysis relied on 50 Hz data and on a study-specific shoulder-to-pelvis anthropometric approximation that was not independently validated. Event localisation therefore has an uncertainty of approximately one video frame (20 ms), and the downstream kinematic quantities were not concurrently validated; these results should remain hypothesis-generating and should not support millisecond-level mechanistic interpretation. Eighth, trials were classified by whether the return produced a legal landing, without further distinguishing within-table landing accuracy, so differences in performance quality may still exist within the successful trials.

Conclusions

Within the same standardised forehand-drive task, failed trials were mainly characterised by higher anteroposterior and vertical ground reaction forces and by greater combined-COP movement speed, path length and mediolateral fluctuation; as a secondary result, the force-peak timing suggested that anteroposterior support-force peak timing may be altered, with interpretation limited by the temporal resolution of the 50 frames/s movement window. The added sensitivity analyses showed that the direction of the core GRF/COP effects was generally consistent across exclusion of participants who contributed

successful trials only, body-weight-normalised GRF models and multiple contact-related windows, although some short-window effect sizes were reduced, indicating that the main GRF/COP pattern is most appropriately viewed as observational evidence from amateur forehand-drive trials, constrained by window length and sample size.

Abbreviations

AP
anteroposterior
BW
body weight
CI
confidence interval
COM
centre of mass
COP
centre of pressure
EMM
estimated marginal mean
FDR
false discovery rate
Fx
summed bilateral anteroposterior ground reaction force
Fy
summed bilateral mediolateral ground reaction force
Fz
summed bilateral vertical ground reaction force
Fz2
left-foot vertical ground reaction force recorded by plate 2
GRF
ground reaction force
LMM
linear mixed model
ML
mediolateral
RMS
root mean square
SMD
standardised mean difference.

Declarations

Ethics approval and consent to participate

This study was approved by the Ethics Committee of South China Normal University (approval number: SCNU-SPT-2023-037) and was conducted in accordance with the Declaration of Helsinki. All participants provided written informed consent before participation.

Consent for publication

Consent to Publish declaration: not applicable.

Competing interests

The authors declare that they have no competing interests.

Use of artificial intelligence

Generative AI was used only for English-language editing and formatting checks. It was not used for study design, data collection, data processing, statistical analysis, figure generation or scientific interpretation. All authors reviewed and approved the final manuscript and take full responsibility for its content.

Additional file

Additional file 1 (.docx): Supplementary tables. Table S1, participant trial contributions; Table S2, full trial-level LMM results for the 30 prespecified GRF/COP indicators; Table S3, contact-related-window sensitivity summary; Table S4, body-weight-normalised GRF sensitivity analyses; Table S5, FDR-significant exploratory markerless kinematic indicators; Table S6, full contact-window sensitivity results for all 30 GRF/COP indicators; Table S7, sex-adjusted sensitivity analysis for all 30 primary GRF/COP models.

Funding

This research received no specific grant from any funding agency in the public, commercial or not-for-profit sectors.

Author Contribution

M.H. Y.S. contributed to conceptualisation, methodology, investigation, data curation, formal analysis, visualisation and writing the original draft. L.M. contributed to conceptualisation, supervision, project administration, interpretation of the findings and writing, review and editing. Y.D. and K.X. contributed to data curation and data checking. C.D. contributed to investigation and experimental assistance. L.W. contributed to conceptualisation, supervision, project administration, interpretation of the findings and writing, review and editing. All authors read and approved the final manuscript.

Acknowledgement

The authors thank the participants for their time and effort during data collection.

Data Availability

The de-identified analysis dataset and analysis code supporting the findings of this study are available from the corresponding author upon reasonable request. Raw video files, markerless motion-capture files and force-plate source files are not publicly available because they may contain information that could compromise participant privacy and because of their large file size.

References

1. Bańkosz Z, Winiarski S. Correlations between angular velocities in selected joints and velocity of table tennis racket during topspin forehand and backhand. J Sports Sci Med. 2018;17(2):330–8.
2. Iino Y. Hip joint kinetics in the table tennis topspin forehand: relationship to racket velocity. J Sports Sci. 2018;36(7):834–42. 10.1080/02640414.2017.1344777.
3. Iino Y, Mori T, Kojima T. Contributions of upper limb rotations to racket velocity in table tennis backhands against topspin and backspin. J Sports Sci. 2008;26(3):287–93. 10.1080/02640410701501705.

4. Iino Y, Kojima T. Kinetics of the upper limb during table tennis topspin forehands in advanced and intermediate players. Sports Biomech. 2011;10(4):361–77. 10.1080/14763141.2011.629304.
5. He Y, Lyu X, Sun D, Baker JS, Gu Y. The kinematic analysis of the lower limb during topspin forehand loop between different level table tennis athletes. PeerJ. 2021;9:e10841. 10.7717/peerj.10841.
6. He Y, Liang M, Fang Y, Fekete G, Baker JS, Gu Y. Lumbar and pelvis movement comparison between cross-court and long-line topspin forehand in table tennis: based on musculoskeletal model. Front Bioeng Biotechnol. 2023;11:1185177. 10.3389/fbioe.2023.1185177.
7. Zhu R, Yang X, Chong LC, Shao S, István B, Gu Y. Biomechanics of topspin forehand loop in table tennis: an application of OpenSim musculoskeletal modelling. Healthc (Basel). 2023;11(9):1216. 10.3390/healthcare11091216.
8. Iino Y, Kojima T. Kinematics of table tennis topspin forehands: effects of performance level and ball spin. J Sports Sci. 2009;27(12):1311–21. 10.1080/02640410903264458.
9. Wang M, Fu L, Gu Y, Mei Q, Fu F, Fernandez J. Comparative study of kinematics and muscle activity between elite and amateur table tennis players during topspin loop against backspin movements. J Hum Kinet. 2018;64(1):25–33. 10.1515/hukin-2017-0182.
10. Li Z, Wang L, Zhang L, Hou Y, Sun Y. Effects of loop type and target direction variation on kinematics and kinetics of table tennis backhand loop: a statistical parametric mapping approach. Front Bioeng Biotechnol. 2025;13:1722210. 10.3389/fbioe.2025.1722210.
11. Malagoli Lanzoni I, Bartolomei S, Di Michele R, Fantozzi S. A kinematic comparison between long-line and cross-court top spin forehand in competitive table tennis players. J Sports Sci. 2018;36(23):2637–43. 10.1080/02640414.2018.1456394.
12. He Y, Lv X, Zhou Z, Sun D, Baker JS, Gu Y. Comparing the kinematic characteristics of the lower limbs in table tennis: differences between diagonal and straight shots using the forehand loop. J Sports Sci Med. 2020;19(3):522–8.
13. Jin P, Yang C, Bańkosz Z, Sun B, Kong Q, Ren J. Kinetics of lower limb joints during forehand loops with alternating and full-foot support patterns in table tennis. Sports Biomech. 2026. 10.1080/14763141.2026.2664127.
14. Yang X, Mei Q, Shao S, Gu W, He Y, Zhu R, et al. Understanding sex-based kinematic and kinetic differences of chasse-step in elite table tennis athletes. Bioeng (Basel). 2022;9(6):246. 10.3390/bioengineering9060246.
15. Yang X, Wang Y, Mei Q, Shao S, Gu Y, Fernandez J. Chasse-step and one-step footwork reported different biomechanical profiles in elite table tennis athletes. J Sports Sci Med. 2025;24(2):453–62. 10.52082/jssm.2025.453.
16. Yu C, Shao S, Baker JS, Gu Y. Comparing the biomechanical characteristics between squat and standing serves in female table tennis athletes. PeerJ. 2018;6:e4760. 10.7717/peerj.4760.
17. He Y, Fekete G, Sun D, Baker JS, Shao S, Gu Y. Lower limb biomechanics during the topspin forehand in table tennis: a systemic review. Bioeng (Basel). 2022;9(8):336. 10.3390/bioengineering9080336.
18. Yu C, Shao S, Awrejcewicz J, Baker JS, Gu Y. Lower limb maneuver investigation of chasse steps among male elite table tennis players. Med (Kaunas). 2019;55(4):97. 10.3390/medicina55040097.
19. Bańkosz Z, Winiarski S, Malagoli Lanzoni I. Gender differences in kinematic parameters of topspin forehand and backhand in table tennis. Int J Environ Res Public Health. 2020;17(16):5742. 10.3390/ijerph17165742.
20. Zhang J, Ren Y, Lin L, Xing Y, Ren J. Table tennis motion recognition based on the bat trajectory using varying-length-input convolution neural networks. Sci Rep. 2024;14(1):3549. 10.1038/s41598-024-54150-5.
21. Elliott B. Biomechanics and tennis. Br J Sports Med. 2006;40(5):392–6. 10.1136/bjsm.2005.023150.
22. Liu H, Li HJ, Qu Y, He XG, Zhou ZP, Yu B. Validity of an artificial intelligence system for markerless human movement automatic capture. J Beijing Sport Univ. 2021;44(1):125–33. 10.19582/j.cnki.11-3785/g8.2021.01.014.
23. Kanko RM, Laende EK, Davis EM, Selbie WS, Deluzio KJ. Concurrent assessment of gait kinematics using marker-based and markerless motion capture. J Biomech. 2021;127:110665. 10.1016/j.jbiomech.2021.110665.
24. Nakano N, Sakura T, Ueda K, Omura L, Kimura A, Iino Y, et al. Evaluation of 3D markerless motion capture accuracy using OpenPose with multiple video cameras. Front Sports Act Living. 2020;2:50. 10.3389/fspor.2020.00050.

25. Uhlrich SD, Falisse A, Kidziński Ł, Muccini J, Ko M, Chaudhari AS, et al. OpenCap: human movement dynamics from smartphone videos. PLoS Comput Biol. 2023;19(10):e1011462. 10.1371/journal.pcbi.1011462.
26. Lyu Y, Duan X, Yang C, Ye Q. Development of a MediaPipe-based framework for biomechanical quantification of table tennis forehand strokes. Front Sports Act Living. 2025;7:1635581. 10.3389/fspor.2025.1635581.
27. Bańkosz Z, Winiarski S. Using wearable inertial sensors to estimate kinematic parameters and variability in the table tennis topspin forehand stroke. Appl Bionics Biomech. 2020;2020:8413948. 10.1155/2020/8413948.
28. Tian J, Xiao Y. Research on the difference of stroke characteristics and stroke effect between different stroke duration of table tennis players. Sci Rep. 2024;14(1):25405. 10.1038/s41598-024-76802-2.
29. Robertson DGE, Caldwell GE, Hamill J, Kamen G, Whittlesey SN. Research methods in biomechanics. 2nd ed. Champaign, IL: Human Kinetics; 2014.
30. Winter DA. Biomechanics and motor control of human movement. 4th ed. Hoboken, NJ: Wiley; 2009.
31. He Y, Sun D, Yang X, Fekete G, Baker JS, Gu Y. Lower limb kinetic comparisons between the chasse step and one step footwork during stroke play in table tennis. PeerJ. 2021;9:e12481. 10.7717/peerj.12481.
32. Delp SL, Anderson FC, Arnold AS, Loan P, Habib A, John CT, et al. OpenSim: open-source software to create and analyze dynamic simulations of movement. IEEE Trans Biomed Eng. 2007;54(11):1940–50. 10.1109/TBME.2007.901024.
33. Hicks JL, Uchida TK, Seth A, Rajagopal A, Delp SL. Is my model good enough? Best practices for verification and validation of musculoskeletal models and simulations of movement. J Biomech Eng. 2015;137(2):020905. 10.1115/1.4029304.
34. Bell AL, Pedersen DR, Brand RA. A comparison of the accuracy of several hip center location prediction methods. J Biomech. 1990;23(6):617–21. 10.1016/0021-9290(90)90054-7.
35. de Leva P. Adjustments to Zatsiorsky-Seluyanov's segment inertia parameters. J Biomech. 1996;29(9):1223–30. 10.1016/0021-9290(95)00178-6.
36. Pinheiro JC, Bates DM. Mixed-effects models in S and S-PLUS. New York, NY: Springer; 2000.
37. JASP Team. JASP (Version 0.97.0) [Computer software]. 2026.
38. Bates D, Mächler M, Bolker B, Walker S. Fitting linear mixed-effects models using lme4. J Stat Softw. 2015;67(1):1–48. 10.18637/jss.v067.i01.
39. Kuznetsova A, Brockhoff PB, Christensen RHB. lmerTest package: tests in linear mixed effects models. J Stat Softw. 2017;82(13):1–26. 10.18637/jss.v082.i13.
40. Benjamini Y, Hochberg Y. Controlling the false discovery rate: a practical and powerful approach to multiple testing. J R Stat Soc Ser B Stat Methodol. 1995;57(1):289–300. 10.1111/j.2517-6161.1995.tb02031.x.
41. Lenth RV, Piaskowski J. emmeans: estimated marginal means, aka least-squares means. R package version 2.0.3. 2026. 10.32614/CRAN.package.emmeans
42. Cohen J. Statistical power analysis for the behavioral sciences. 2nd ed. Hillsdale, NJ: Lawrence Erlbaum Associates; 1988.

Figures

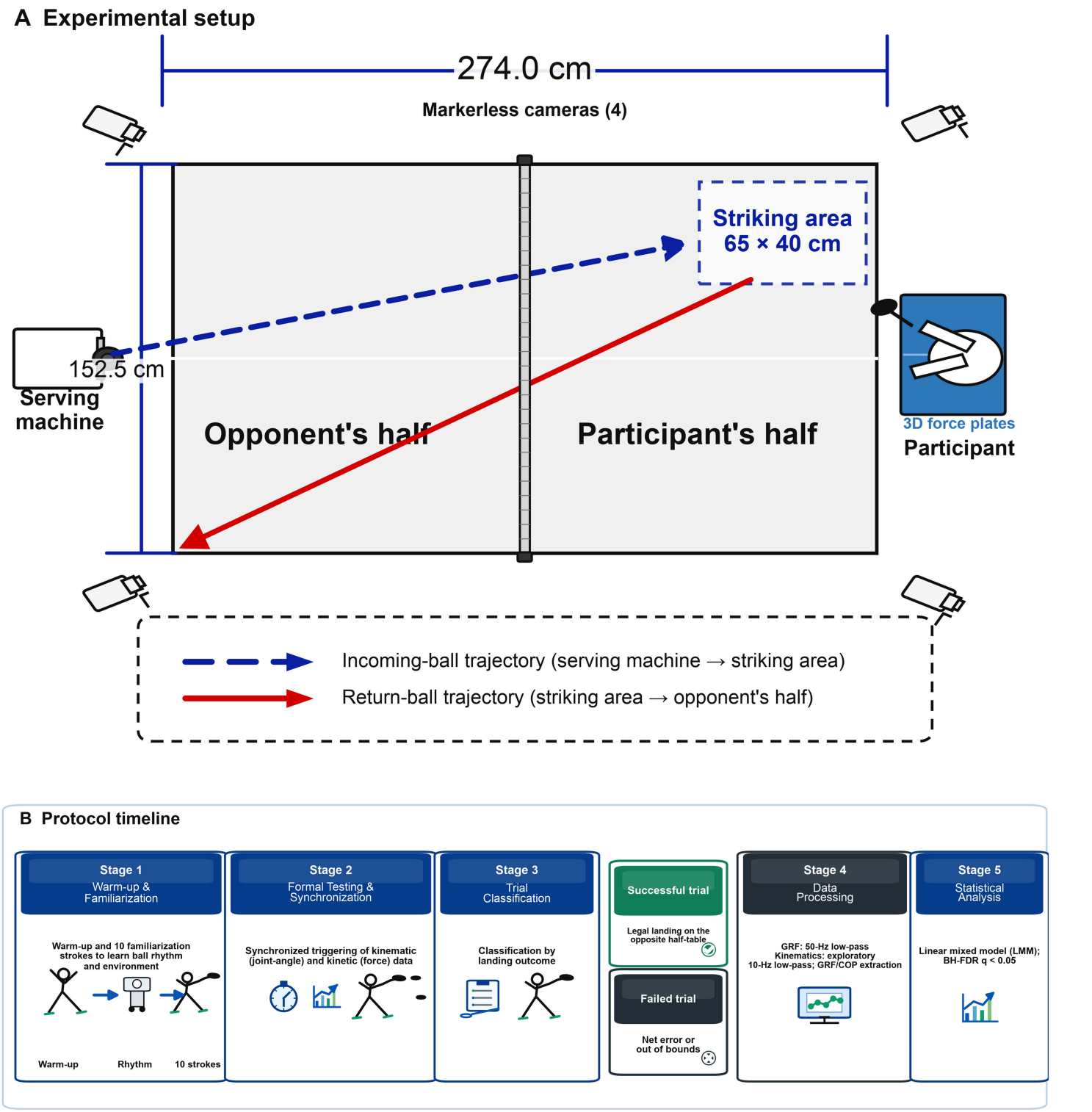


Figure 1

Experimental setup and protocol. (A) A table-tennis serving machine was placed at one end of the table and delivered topspin balls to the participant's striking area; the participant returned the ball with a forehand drive to the opposite half of the table. The blue dashed line and the red solid line denote the incoming-ball and return-ball trajectories, respectively, and the dimensions of the striking area (65 cm × 40 cm) are annotated. (B) Protocol timeline from warm-up and familiarisation to formal testing, trial classification, data processing and statistical analysis.

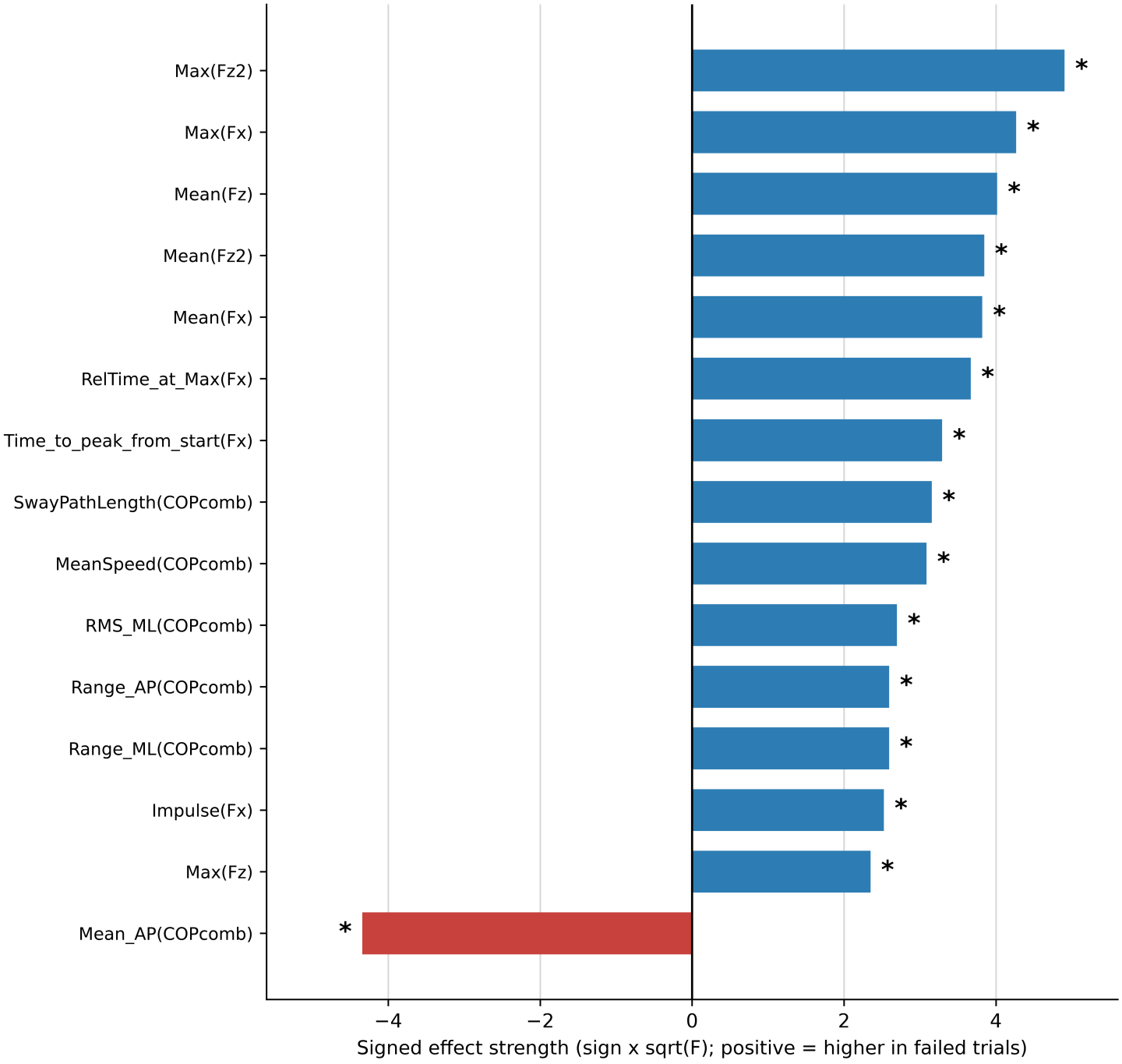


Figure 2

Signed visualisation of the fixed-effect F statistics for kinetic and COP indicators. The horizontal axis is sign × √F, with positive values indicating higher values in failed trials; this transformation is a signed visualisation of the F statistic and is not a standardised effect-size measure. "*" denotes q < 0.05 after FDR correction. Blue bars indicate higher or later values in failed trials, and red bars indicate lower values in failed trials. Fx, Fy and Fz are the summed bilateral anteroposterior, mediolateral and vertical ground reaction forces; Fz2 is the left-foot vertical force recorded by plate 2; and COPcomb is the combined centre of pressure of the two feet.

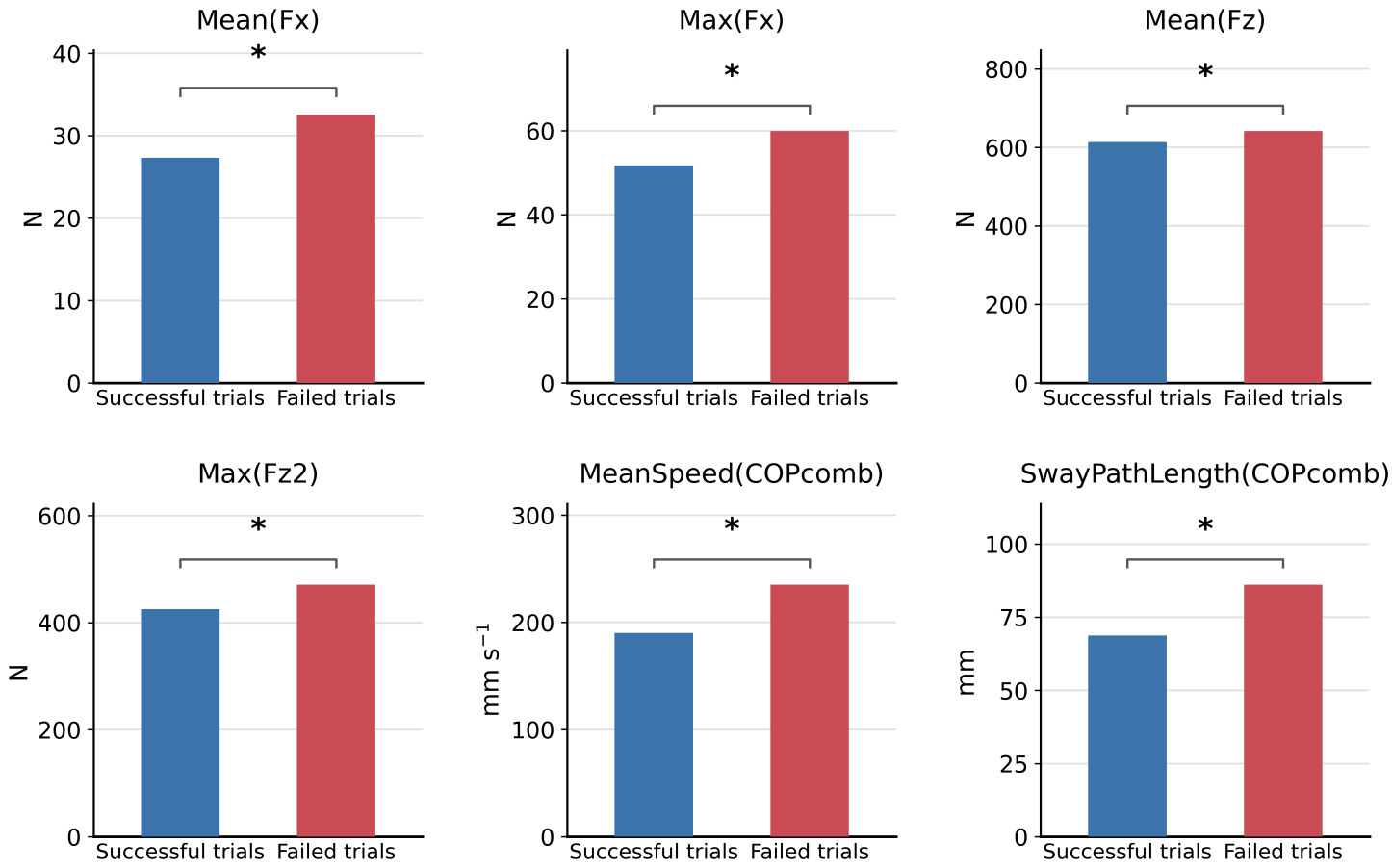


Figure 3

Estimated marginal means of key kinetic and COP indicators. Blue denotes successful trials and red denotes failed trials; "*" denotes $q < 0.05$ after FDR correction. Bars represent estimated marginal means; corresponding 95% confidence intervals are reported in Table 1. Vertical-axis units: N for force, mm·s⁻¹ for COP speed, and mm for COP path length.

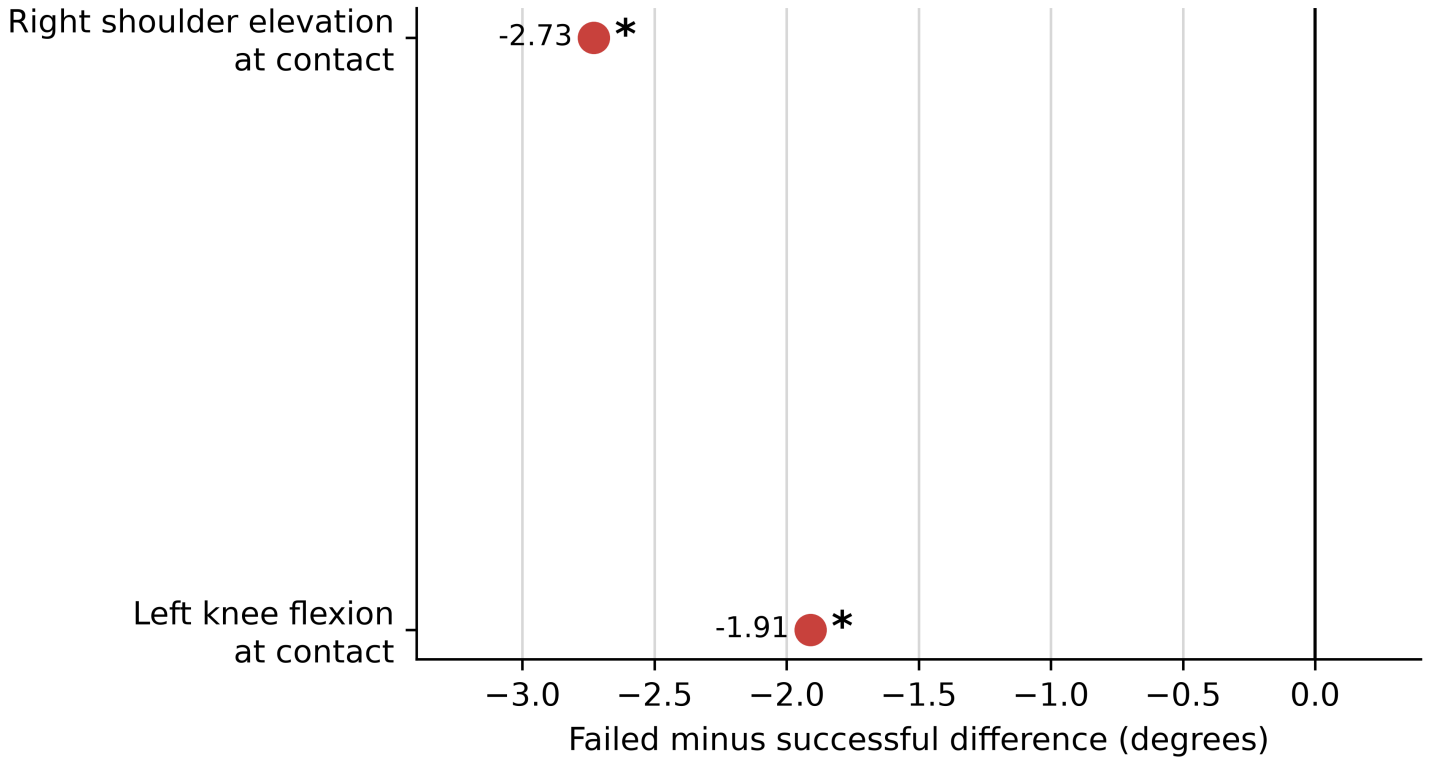


Figure 4

Contact-related kinematic differences. Points show the observed failed-minus-successful mean differences reported in Table 2; red denotes q < 0.05 after FDR correction. Differences are shown in degrees.

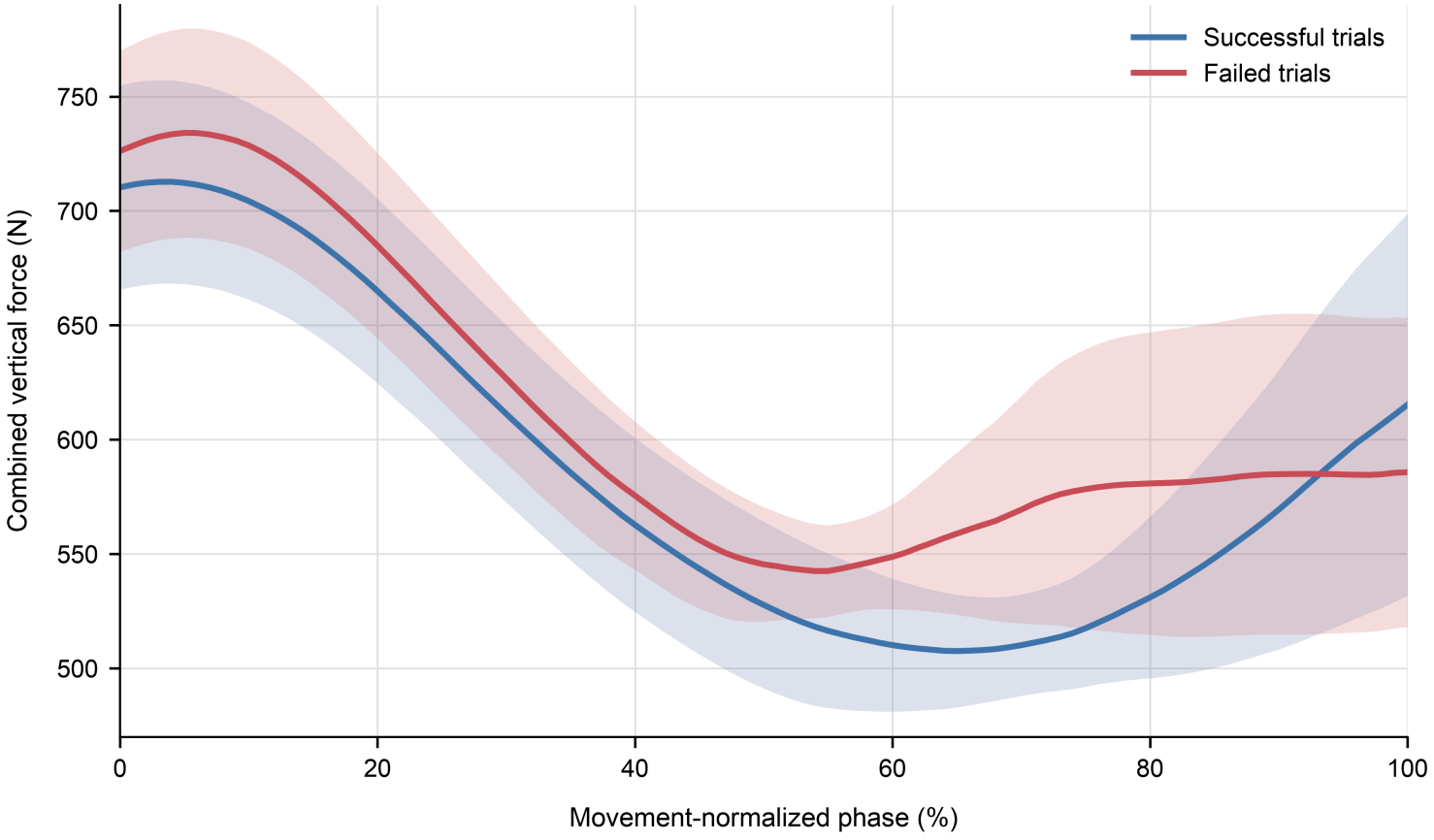


Figure 5

Combined vertical support-force phase curves. The curves compare successful and failed trials among participants who contributed both outcome types. The horizontal axis is the normalised movement phase (%) and the vertical axis is the combined vertical force (N); solid lines denote participant-level mean curves and shading denotes the standard error (SE) across participants.

Supplementary Files

This is a list of supplementary files associated with this preprint. Click to download.

- Additionalfile1supplementarytables.docx